Magnetic Interactions in Supramolecular NO···HC ⋮ C Type Hydrogen-Bonded Nitronylnitroxide Radical Chains

ARTICLE *in* THE JOURNAL OF PHYSICAL CHEMISTRY B · MAY 2007

Impact Factor: 3.3 · DOI: 10.1021/jp066605k · Source: PubMed

4 AUTHORS, INCLUDING:

Rajadurai Chandrasekar
University of Hyderabad
68 PUBLICATIONS **1,076** CITATIONS
SEE PROFILE

Giorgio Zoppellaro
Palacký University of Olomouc
74 PUBLICATIONS **1,163** CITATIONS
SEE PROFILE

Martin Baumgarten
Max Planck Institute for Polymer Research
278 PUBLICATIONS **4,243** CITATIONS
SEE PROFILE

Magnetic Interactions in Supramolecular N−O···H−C≡C− Type Hydrogen-Bonded Nitronylnitroxide Radical Chains

Chandrasekar Rajadurai,[†] Volker Enkelmann, Giorgio Zoppellaro,[†] and Martin Baumgarten*

Max Planck Institute for Polymer Research, Ackermannweg 10, D-55128 Mainz, Germany

Received: October 8, 2006; In Final Form: February 3, 2007

Two paramagnetic building blocks, 2-(4-ethynyl-1-phenyl)-4,4,5,5-tetramethylimidazoline-1-oxyl (**3**) and 2-(5-ethynyl-2-pyridyl)-4,4,5,5-tetramethylimidazoline-1-oxyl (**4**) were synthesized and crystallized. Single crystal X-ray studies of **3** and **4** show the formation of supramolecular *head-to-tail* one-dimensional H-bonded (N−**O**···H−**C**≡C− type) chain structures with **O**···**C** distances of 3.181 and 3.155 Å, respectively. High-resolution isotropic liquid state ($c \leq 10^{-4}$ M) electron spin resonance (ESR) spectroscopy studies of the well-isolated molecules confirmed the *intramolecular* spin polarization from the nitronylnitroxide radical group (acceptor, N−**O**) to the acetylenic proton (donor, **H**−C≡C−), which is mediated by the π-conjugated backbone. The influence of the heteroatom (pyridine nitrogen−^{14}N) in the ESR hyperfine splitting pattern was clearly seen in radical **4**, with an additional number of lines appearing in the $M_I = 0$ line of the total five-line spectrum. The solution state paramagnetic ^{1}H NMR investigation of radicals 2-(4-trimethylsilylethynyl-1-phenyl)-4,4,5,5-tetramethylimidazoline-1-oxyl (**1**) and **3** clearly support the *intramolecular* spin density propagation from the acceptor to the donor groups as well as the proton hyperfine coupling (hfc) values of the conjugated backbone determined by ESR studies. Bulk magnetic investigations of the polycrystalline chain compounds (**3** and **4**) in the temperature range 300 down to 4.5 K display antiferromagnetic exchange interactions at very low temperature. The experimental bulk magnetic data were found to be fit by using the dimer model with exchange coupling $2J/K_B$ values of -3.10 ± 1.16 and -8.00 ± 3.83 K for **3** and **4**, respectively, as well as by adopting the Heisenberg-chain model with $2J/K_B$ values of -0.62 ± 0.02 and -2.21 ± 0.13 K for **3** and **4**, respectively.

Introduction

The search for paramagnetic organic molecules, which form supramolecular and macromolecular architectures, challenges both theoretical and synthetic design.[1−12] In this context, two guiding principles have been followed so far, namely, the *covalent* and *noncovalent* approach. Rajca and co-workers followed the former approach, which is based on Gomberg's triarylmethyl radical, and synthesized both high-spin macrocyclic molecules and organic magnetic polymers of spin value up to $S = 5000$.[1g−j] In the *noncovalent* (supramolecular) approach, H-bonding[1a−f,8,11] or $\pi-\pi$ interactions[9−11] provide complementary methods for generating supramolecular networks in the solid state starting from simple paramagnetic building blocks, although most of the reported results on bulk ferromagnetism are still based on serendipity. Thus, a thorough understanding of the magnetic properties and further development of pure organic molecule based magnets requires model systems, which assemble in the crystalline state utilizing directional interactions ("*crystal engineering*" approach).[12] From the theoretical perspective, the bulk magnetic property of magnetic material mainly originates from the interplay of two mechanisms, (i) intramolecular and (ii) intermolecular spin−spin interactions, although the (exchange coupling constant *J*) sign and strengths of such interactions vary depending on the molecular and crystal structures. A convenient way to verify the *intramolecular* spin density distribution or "π-spin polarization effect" in a paramagnetic molecule is by studying the well-resolved M_I lines of the radical obtained by liquid state electron spin resonance (ESR) or electron−nuclear double resonance (ENDOR) spectroscopy under high-resolution conditions.[13−16] Alternatively, both the sign and magnitude of the spin densities in organic radicals can be probed through ^{1}H NMR spectroscopic studies.[11,17−20]

Even though the spin density distribution pathways can be revealed using the above techniques, it is still difficult to forecast the consequential bulk magnetic properties of pure organic radical crystals. For this purpose, the McConnell-I mechanism has been widely applied in the design and magnetostructural analysis of paramagnetic organic crystals.[31] However, the statistical analysis made by Novoa et al. on the structure−magnetism relationship for several α-nitronylnitroxide (NIT) (where the SOMO is localized on the O−N−C−N−O chain of the NIT) based organic crystal systems showed that defining clearly the magnetic role associated with the N−O···O−N and N−O···H−C contacts still seems unfeasible.[21,22] This study underlines the importance of considering all of the magnetically active intermolecular short contacts in the solid state. Hence magnetic interactions mediated through space are still a subject of great interest, particularly in the H-bonded systems in order to identify the magnetic role of the noncovalent interaction. Recently, Romero et al.[5,6] have studied H-bonded meta-pyridine ethynyl based nitronyl and iminonitroxide systems, where ferromagnetic behavior was observed and the **intermolecular** polarization (*spin density transfer through H-bonds*) of spin densities to acetylenic protons in a chain was demonstrated by polarized neutron diffraction studies. However, it is still

* Corresponding author. Phone: (+49) 06131−379142. Fax: (+49) 06131−379 370. E-mail: baumgart@mpip-mainz.mpg.de.

[†] Current Address: Institute of Nanotechnology, Forschungszentrum Karlsruhe, Helmholtz−Gemeinschaft 76021, Germany. Phone: (+49) 06131−379142. Fax: (+49) 06131−379370. E-mail: baumgart@mpip-mainz.mpg.de.

10.1021/jp066605k CCC: $37.00
Published on Web 04/12/2007

SCHEME 1: Chemical Structures of Trimethylsilyl Protected (1 and 2) and Trimethylsilyl Deprotected (3 and 4) Monoradicals

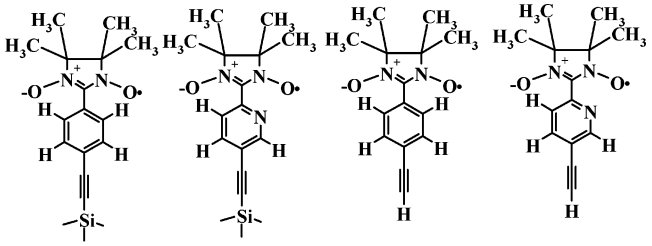

important to understand the operating **intramolecular** spin polarization mechanism of an isolated molecule in solution in order to probe the electronic importance of H-bonds in the solid state. Especially, the knowledge of the intramolecular spin density distribution on the H-donor group is vital to recognize the magnetic coupling between the molecules in the crystalline state.

We have synthesized and crystallized two H-bonding $S = {}^1/_2$ building blocks (Scheme 1), namely, 2-(4-ethynyl-1-phenyl)-4,4,5,5-tetramethylimidazoline-1-oxyl (**3**) and 2-(5-ethynyl-2-pyridyl)-4,4,5,5-tetramethylimidazoline-1-oxyl (**4**). These two molecules form supramolecular hydrogen-bonded chain structures in the crystalline state. The aim of the work was to probe the influence of aryl connectors and the para substitution on the magnetic properties of randomly distributed molecules (without H-bonding) in the *solution state* and ordered molecules (with H-bonding) in the *crystalline state*. In these molecules the nitronyl nitroxide radical and the acetylenic groups are attached to the connectors (benzene and pyridine) with respect to each other in the para position (1,4-substituted) in order to carry positive spin densities (↑) on the radical oxygen (O-acceptor) and the acetylenic hydrogen (H-donor). In this article, we present the synthesis of monoradicals **3** and **4**, their X-ray structures, evidence of intramolecular spin polarization by high-resolution fluid state EPR spectroscopy as well as by paramagnetic NMR studies, and their detailed intermolecular magnetic properties in the solid state obtained by bulk magnetometry.

Results and Discussion

1. Synthesis of Monoradical Building Blocks. Building blocks **3** and **4** were prepared by the Sonogashira coupling reaction[23] of trimethylsilylacetylene (TMSA) with corresponding arylbromoaldehydes followed by deprotection of the TMS group and subsequent Ullman's condensation[24] reaction with 2,3-dimethyl-2,3-bis(hydroxylamino)butane followed by oxidation with $NaIO_4$ (Scheme 2). The synthesis of compounds **1**, **2**, **5**, **6**, **8**, and **9** were reported in our previous work.[25] When this manuscript was in preparation, the synthesis of **3** was reported by another group without any further studies.[26] Compound **10** was synthesized from **9** by using K_2CO_3/MeOH in 70% yield. Reaction of **6** and **10** with 2,3-dimethyl-2,3-bis(hydroxylamino)-butane in dichloromethane and methanol afforded the corresponding condensation products **7** and **11** as white precipitates. Monoradicals **3** and **4** were then obtained by oxidation of the corresponding diamagnetic precursors with $NaIO_4$ under phase transfer conditions (dichloromethane/water). Radicals were purified by column chromatography on silica, and the complete oxidation of the condensation products was confirmed by fast atom bombardment (FAB) mass spectrometric analysis, $m/z = 258$ (calcd 258) and $m/z = 259$ (calcd 259) for **3** and **4**,

SCHEME 2: Reagents and Conditions: (a) Trimethylsilylacetylene (TMSA)/$Pd(PPh_3)_2Cl_2$/CuI/Et_3N/THF, (b) K_2CO_3/MeOH, (c) 2,3-Dimethyl-2,3-bis(hydroxylamino)butane/MeOH/THF, (d) $NaIO_4$/$CHCl_3$/H_2O, (e) *n*-BuLi/Toluene/DMF/−78 °C

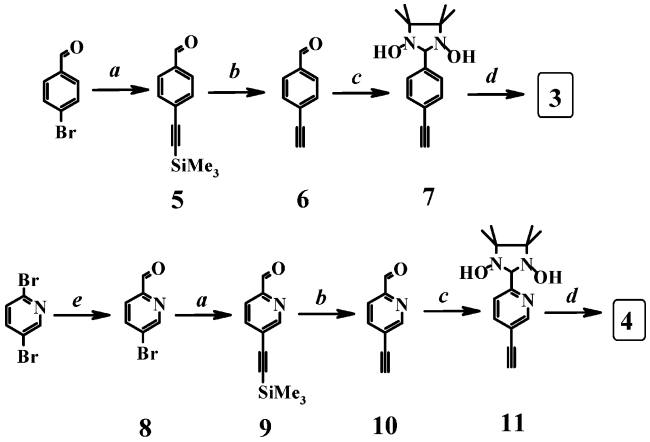

respectively. Single crystals suitable for X-ray and magnetic studies were obtained by crystallizing the radicals (**3** and **4**) from the mixed solvent of petroleum ether (bp 30−40 °C) and acetone (1:1) to afford blue-colored needles.

2. Solid State Structures. The crystal structures of **3** and **4** were obtained by single crystal X-ray crystallography (Figures 1 and 2), which shows both radicals are in monoclinic $P2_1/c$ and orthorhombic *Pbca* space groups, respectively. Each monoradical is connected through weak intermolecular hydrogen bonding between the acetylenic hydrogen and the NIT oxygen of the neighboring molecule (N−O···H−C≡C−), forming supramolecular *head-to-tail* one-dimensional chain structures. The radical chains are propagating in alternating direction, along the crystallographic *b*- and *c*-axis with **O···C** distances of 3.181 Å in **3** and 3.155 Å and **4** (Figure 2). In **3**, the five-membered imidazole ring is planar and all of the methyl groups are in eclipsed conformation. The five-membered ring plane is twisted from the benzene plane by an angle of $\theta_1 = 21.71°$. In contrast, the five-membered imidazole ring of **4** is nonplanar, with the slightly staggered conformation of the four methyl groups and the imidazole ring is twisted from the pyridine plane with an angle of $\theta_2 = 51.61°$. Notably, in **3**, the two N−O bond distances are significantly different. The one participating in the H-bonding (N1−O1 = 1.2856(2) Å) is longer than the other (N2−O2 = 1.2795(2) Å), while, in **4**, the N−O distances are almost equal but longer than those found in **3**. The H-bond forming N3−O2 group distance is 1.2894(2) Å, and the other N2−O1 group distance is 1.2880(2) Å. The reason for these close values is attributed to the existence of short intermolecular contacts of N2−O1 oxygen with two different methyl hydrogens (H113 and H123), as shown in Figure 5.

3. Magnetic Properties. *Intramolecular (Solution State) Magnetic Properties.* The high-resolution isotropic fluid state ESR (X-band) spectra of the intermolecularly isolated ($c \ll 10^{-4}$ M) monoradical building blocks **1**−**4** recorded in degassed toluene/isopropanol solvent mixture at room temperature are shown in Figure 3. They exhibit a well-resolved five-line pattern ($\Delta ms = \pm 1$ transitions) with the nitrogen hyperfine coupling (hfc) values of $a_N = 7.40$, 7.36, 7.47, and 7.44 G, respectively, with an intensity ratio of 1:2:3:2:1 due to the coupling of the unpaired electron of the nitronylnitroxide radical with two equivalent ^{14}N nuclei. Additionally, each of the five lines ($M_I = +2, +1, 0, -1, -2$) are composed of a group of lines due to further hfc with magnetically active nuclei of small spin

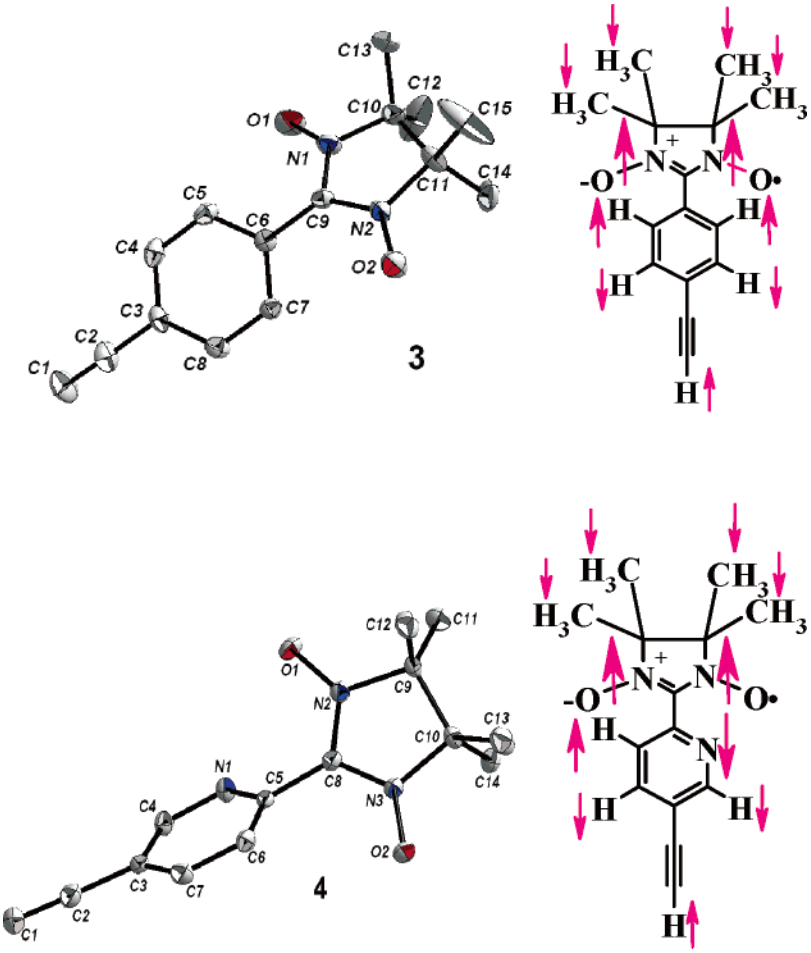

Figure 1. ORTEP view (50% probability thermal ellipsoids) of building blocks **3** and **4** (left) with the atomic numbering used in the main text (hydrogen atoms are omitted for clarity). Chemical structures of the H-bonding building blocks **3** and **4** (right); arrows indicate the spin polarization pathways and their signs (up, positive; down, negative).

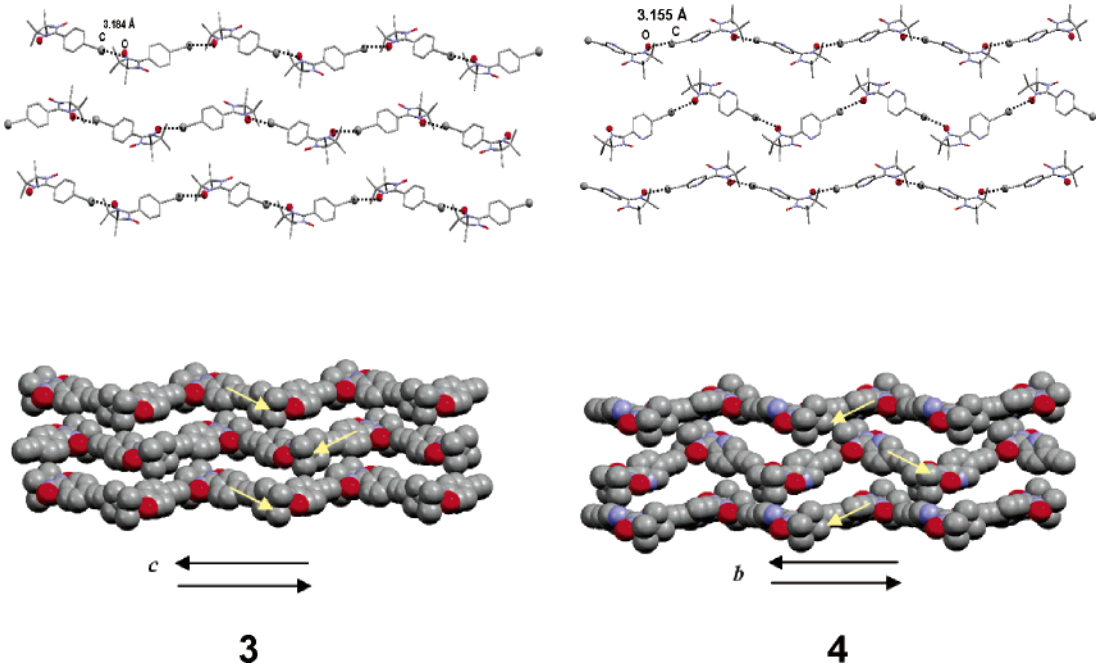

Figure 2. Crystallographic projection of supramolecular chains in capped sticks model, intermolecular *head-to-tail* 1-D H-bonded chains running along the *c*- and *b*-axis for **3** and **4**, respectively (top figures). Their space fill models labeled with light yellow arrows showing the alternating chain propagation directions (bottom figures).

densities. The spectra are recorded at low microwave power (5 mW) in order to avoid saturation of the proton hyperfine splitting. Figure 3 shows the spectra of **1**−**4** obtained under high-resolution conditions together with the simulation of M_I

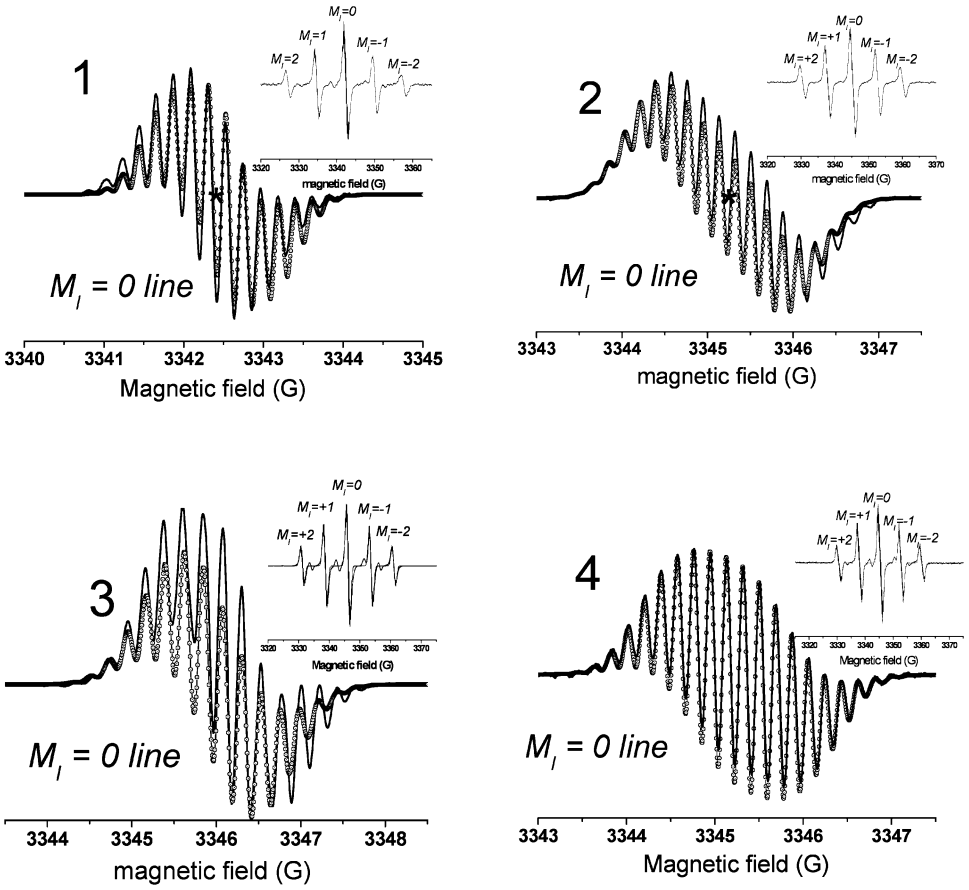

Figure 3. High-resolution isotropic EPR spectra ($\Delta ms = \pm 1$ transitions) of the building block radicals **1**−**4** for the $M_I = 0$ lines, recorded with the following parameters: $c \leq 10^{-4}$ M in a toluene/isopropanol mixture, 6 scans, 293 K, and 0.5 mW microwave power. Asterisks show the central magnetic field position. The solid lines (—) show the experimental spectra, and the dotted lines (-○-) show the computer simulated spectra. The insets show the corresponding resolved total five-line spectra.

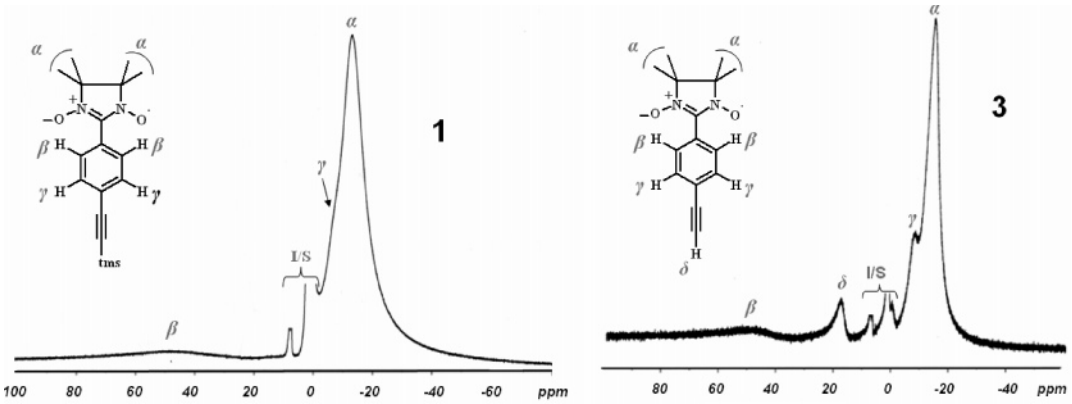

Figure 4. Paramagnetic ^{1}H NMR (300 MHz) spectra of radical building blocks **1** and **3** in $CDCl_3$ solvent at room temperature with the labeling of protons (α, β, γ, and δ). S = solvent, I = diamagnetic impurities.

= 0 lines. A close investigation of the central group of lines ($M_I = 0$) in the five-line spectra revealed the spin polarization pathways in **1**−**4**. Interestingly, in **1**, the central magnetic field is in the middle of a single line (marked by *), due to the benzene protons, where only $I = {}^1/_2$ nuclei participates in hfc. While for **2** in comparison with **1**, the central field is in the middle of two lines due to the modulation of the spin polarization path, which arises from the participation of the pyridine nitrogen ($I = 1$) nuclei instead of a proton ($I = {}^1/_2$) as in **1**. In addition, the total width of the $M_I = 0$ line in the case of **2** is much broader (4.0 G) than that of **1** (3.58 G) with additional lines due to the strong pyridine nitrogen ($I = 1$) influence on the spin density distribution causing extra splittings and line broadening. The major group in the central line ($M_I =$ 0) of the spectra of radicals (**1**−**4**) were best simulated,[27] and the hfc values are presented in Table 1. Particularly, as expected, the simulated spectrum of **2** shows two types of meta protons (hfc constants: $a_H = 0.16$ and 0.21 G) in comparsion with radical **1** ($a_H = 0.17$ G). Analysis of the spectra of radicals **3** and **4** confirms that the spin density is distributed throughout the conjugated backbone from the nitronyl nitroxide moiety. Particularly, comparison of the spectrum of radical **3** with **1** and **4** with **2** revealed extra splittings, which is further confirmed by an increase in the total line width. This arises from the contribution of the additional coupling of the alkyne protons. The simulated hfc values of the H-bond donor alkyne protons ($a_{C\equiv H}$) are 0.20 and 0.18 G, respectively, for **3** and **4**. Overall, the above experimental spectra clearly demonstrate the intramo-

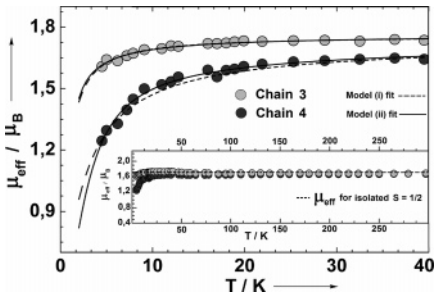

Figure 5. Experimental magnetic behavior of randomly oriented polycrystalline samples of **3** (gray circles) and **4** (black circles) recorded in the low-temperature region. The dashed and solid lines represent the best fit obtained by using the dimer model (model i) and the Heisenberg-chain model (model ii), respectively. The inset shows the overall magnetic trend of **3** (gray circles) and **4** (black circles) in the temperature range 300 down to 4.5 K.

TABLE 1: Isotropic Hyperfine Coupling (hfc) Constants Found for Building Blocks 1−4 Using ESR[a] and NMR Techniques[b]

radical	a_{Me}	$a_{H\ ortho}$	$a_{H\ meta}$	a_N	$a_{C\equiv H}$	method
1	0.20	0.49	0.17			ESR
2	0.18	0.38	0.16 and 0.21	0.54		ESR
3	0.20	0.48	0.22		0.20	ESR
4	0.19	0.33	0.18 and 0.20	0.54	0.18	ESR
1	+0.1913	+0.5041				NMR
3	+0.1908	+0.5135	-0.2113		+0.2033	NMR

[a] Calculated by the computer simulation of the experimental spectra. [b] The hfc constant values are in Gauss units, and the experimental data were collected at room temperature.

lecular spin wave propagation from the **O**−**N**−C−**N**−**O** functionality to the alkyne protons via two different spin density modulating units (benzene and pyridine).

To detect both the sign and magnitude of proton hfc constants of paramagnetic compounds, the nuclear magnetic resonance technique has been widely used as an alternative tool to electron−nuclear double resonance (ENDOR) studies.[11,17−20] In concentrated radical solutions, due to the very rapid spin exchange, a shift in the resonance lines occurs together with the line broadening. These lines are broadened by the relaxation of proton spin in the presence of electron spin. Such shifts are observed only in paramagnetic molecules and arise by virtue of the Fermi contact unpaired electron spin-nuclear spin hyperfine coupling, according to eq 1, where a is the

$$a = (8\pi/6S)g_e\beta_e g_N\beta_N|\psi(0)|^2 \qquad (1)$$

hyperfine coupling constant, in ergs. g_e and g_N are electron and nuclear g values, respectively, β_e and β_N are Bohr and nuclear magnetons, respectively, and $\psi(0)$ is the molecular wave function evaluated at the nuclear position. According to Jesson,[18] in the presence of negligible anisotropy with $g_{av} = [(g_{xx} + g_{yy} + g_{zz})/3]$ and $T_1 < \tau_r$, the shift of a given line ($\Delta\upsilon$) is related to the hyperfine interaction (a) by the following equation, where υ is the spectrometer operating

$$\Delta\upsilon = -g_{av}\beta_e S(S+1)\upsilon a/g_N\beta_N 3kT \qquad (2)$$

frequency, S is the total spin, T_1 is the electron relaxation time, and τ_r is the rotational tumbling time of the molecule. In paramagnetic molecules, nuclei carrying positive spin density shift the line downfield and nuclei having negative spin density shift the line upfield. In our studies, the ^{1}H-NMR spectra were recorded using concentrated solutions of **1** and **3** in $CDCl_3$ solvent at room temperature to further identify the acetylenic proton and also to determine both the sign and magnitude of proton hfc constants and the spin densities at the ring carbons (Figure 4). Comparison of the spectra of **1** with **3** clearly shows a new downfield shifted acetylenic proton peak at 18.25 ppm. The line shift values ($\Delta\upsilon = \upsilon_{exp} - \upsilon_{dia}$) of both **1** and **3** were calculated from their diamagnetic precursor chemical shift values. The proton hyperfine coupling constant (a_H) from eq 2 as well as spin densities of the aromatic ring were determined using McConnell's equation ($a = Q\rho_c^{\pi}$; assuming $Q = -22.5$ G ; ρ_c^{π} is the unpaired electron spin density in the carbon p_z orbital). For **1**, the determined values are as follows: the ortho proton (β), $a_H = +0.5041$ G ($\rho_c^{\pi} = -0.0224$); methyl protons (α), $a_H = +0.1913$ G (the meta protons (γ) peak could not be resolved). Compound **3** showed well-resolved lines for all of the protons including the acetylenic proton (δ), and the presence of positive spin density at this proton can be seen from the downfield shifted (δ) peak. The calculated hfc and spin densities are as follows: the ortho proton (β), $a_H = +0.5135$ G ($\rho_c^{\pi} = -0.0228$); the meta proton (γ), $a_H = -0.2113$ G ($\rho_c^{\pi} = +0.0094$); the methyl protons (α), $a_H = +0.1908$ G; the H-bond donor acetylenic proton (δ), $a_{C\equiv H} \approx +0.2033$ G. Regrettably, the paramagnetic NMR studies require highly concentrated solutions, and due to the small quantity of the available sample, we were not able to perform the NMR studies for **2** and **4**, but for **4**, one can suppose the acetylenic proton hfc magnitude in the same range as seen for radical **3** due to the similar structural type. Alternatively, we have used the available large quantity of 2-(4,4,5,5-tetramethyl-3-oxylimidazoline-1-oxide)-5-bromopyridine to identify the meta pyridine protons, and indeed, both compounds have different spin densities in contrast to the benzene derivatives, as seen from the two upfield shifted peaks.[11] This result clearly supports the EPR simulation, where the two different meta proton hfc values were observed for **2** and **4** in comparison with **1** and **3**. The experimentally (NMR) calculated hfc values of radicals **1** and **3** are in close agreement with the computer simulated hfc values of the EPR spectra (Table 1).

4. Solid State Magnetic Properties. The magnetic susceptibility data for the polycrystalline samples **3** and **4** were collected using a Faraday-type balance within the temperature range 300−4.5 K with an applied field of 0.1 T. At 300 K, as shown in Figure 5, the effective magnetic moment (μ_{eff}) values are 1.67 and 1.63 μ_B for **3** and **4**, respectively, which are close to the theoretical value of 1.73 μ_B for an isolated $S = {}^1/_2$ spin system. The reduced μ_{eff} value observed as compared to the theoretically predicted value clearly implies the coexistence of a fraction of a diamagnetic impurity (5% in **4** and 4% in **3**) in the bulk materials. The experimental magnetic moments are almost constant, down to ∼50 K, with 1.69 μ_B for **3** and 1.63 μ_B for **4**. This observation directly suggests that extended magnetic interaction along and between chains should be rather weak, hence in the energy range of a few kelvins. By lowering furthermore the temperature ($T < 40$ K), on the other hand, the μ_{eff} value decreased for both **3** and **4**, with the larger decrement witnessed by **4**. The analyses of the single crystal X-ray structures of the chains (vide infra) revealed the presence of a complex network made by intermolecular contacts; these through-space interactions involve the N−O radical oxygens and the aromatic and acetylenic protons. Therefore, multiple competing interactions both ferro (⇈) and antiferromagnetic (⇅) are present simultaneously, which render the systems difficult to analyze; however, in the low-temperature regime, the dominant interactions observed in the magnetic trends are surely antiferromagnetic. The observed μ_{eff} trends were simulated adopting two different models as described herein: model i

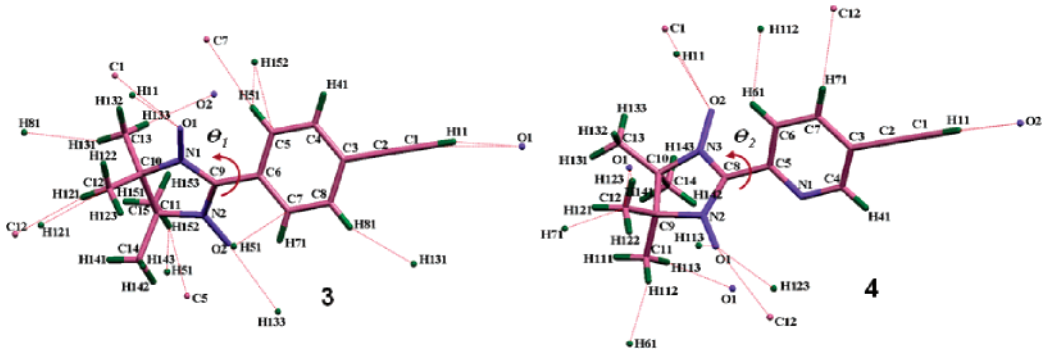

Figure 6. Capped sticks representation of building blocks **3** and **4** with intermolecular contacts and the atomic numbering used in the main text.

breaks the $S = {}^1/_2$ chains into dimeric spin systems ($S = {}^1/_2 - S = {}^1/_2$)[28a−c] in such a way that the susceptibility data can be modeled according to eq 3, where J is the exchange coupling constant, μ_B represents the Bohr magneton, N_A is Avogadro's number, g is the system Lande g-factor, T is the temperature in kelvins, k_B is the Boltzmann constant, and θ (K) represents the averaged intermolecular interactions, under the frame of the mean-field approximation model. Model ii considers extended interaction within the infinite $S = {}^1/_2$ chain spin system, the Heisenberg-chain model, with $A-I$ coefficients ($A = 0.25$, $B = 0.074\,975$, $C = 0.075\,235$, $D = 0.9931$, $E = 0.172\,135$, $F = 0.757\,825$) and θ (K) the averaged interchain interactions, which leads to fit the susceptibility data according to eq 4.

$$\chi_m = \frac{N_A g^2 {\mu_B}^2}{k_B(T-\theta)} \times \left[\frac{\exp(-2J/k_B T)}{1+3\times\exp(-2J/k_B T)}\right] \quad (3)$$

$$\chi_m = \frac{N_A g^2 {\mu_B}^2}{k_B(T-\theta)} \times \left[\frac{A+Bx+Cx^2}{1+Dx+Ex^2+Fx^3}\right] \quad (4)$$

$$\text{where } x = \left|\frac{2J}{k_B T}\right|$$

The dimer-system model (i) provides a fairly large exchange energy of $2J/k_B = -3.10 \pm 1.16$ K and $\theta = -1.87 \pm 0.26$ K for **3** ($R^2 = 0.973$) between adjacent hydrogen-bonded spin units, while in the case of **4** the fitting result converges to $2J/k_B = -8.00 \pm 3.83$ K and $\theta = -6.64 \pm 0.42$ K ($R^2 = 0.964$). The Heisenberg-chain model (ii) supports extended interactions whitin the chain with $2J/k_B = -0.62 \pm 0.02$ K and $\theta = -0.22 \pm 0.02$ K for **3** ($R^2 = 0.979$) and $2J/k_B = -2.21 \pm 0.13$ K with $\theta = -1.08 \pm 0.01$ K for **4** ($R^2 = 0.986$). These results show that antiferromagnetic interactions are as much as 3 times stronger in **4** with respect to **3**.

Furthermore, applying the McConnell-I mechanism[29] on the solid state structural contacts obtained at 120 K shows a total of 16 and 14 intermolecular contacts for **3** and **4**, respectively (see Figure 6 and Table 2). It is important to consider all of the close contacts in the magnetostructural correlation, since the occurrence of spin densities on the protons was clearly unraveled both by liquid state NMR and ESR studies. Overall, molecules **3** and **4** encompass 10 ferromagnetic (FM, both atoms have opposite signs) contacts each, as compared to the 6 antiferromagnetic (AFM, both atoms have the same sign) contacts in **3** and **4**. In both chains, the intermolecular N—O···O—N contacts between the molecules are within distances of 4.452 and 4.480 Å, respectively. Here, very strong AFM interaction is expected according to the McConnell-I mechanism, since the spin density product $\rho_{N-O}\rho_{N-O}$ is higher due to the presence of larger positive spin densities on each N—O group. It is now sensible

TABLE 2: Selected Interatomic Distances (Å) and Bond Lengths (Å) Found in the Supramolecular Chains of 3 and 4

3		sign of interaction[a]
	Interatomic Distances	
H11···O1	2.2451(3)	+···+
H81···H131(Me)[b]	2.989	−···−
H152(Me)···C5	2.843	−···−
H152(Me)···H51	2.287	+···+
H51···C7	2.851	+···−
H133(Me)···O2	2.611	−···+
H121(Me)···C12	2.892	−···+
O2···O1	4.452	+···+
	Bond Lengths	
N1−O1	1.2856(1)	
N2−O2	1.2795(2)	
C1−C2	1.1813(3)	

4		sign of interaction[a]
	Interatomic Distances	
H11···O2	2.2087(3)	+···+
C12···O1	3.178	+···+
H61···H112(Me)	2.375	+···−
H71···C12	2.894	−···+
O2···C1	3.155	+···−
O1···H123(Me)	2.531	+···−
O1···H113(Me)	2.602	+···−
O1···O1	4.480	+···+
	Bond Lengths	
N2−O1	1.2880(9)	
N3−O2	1.2894(2)	
C1−C2	1.1912(3)	

[a] According to the spin polarization model. [b] Me = methyl group.

to attribute AFM coupling for the H-bonded contacts between the N—**O···H**—C≡C— groups along the chains in both **3** and **4** to the contacts between atoms carrying positive spin densities, where the presence of a significant amount of acetylenic proton spin densities were identified by NMR and ESR studies. In addition to that, in both **3** and **4**, the other N—O group (which is not involved in the N—**O···H**—C≡C— type H-bonding) also has its contacts with methyl hydrogens (O2···H133; O1···H123; O1···H113) where the spin densities and the signs are now different between the two participating atoms, favoring ferromagnetic coupling. Thus, in both chains, the two major contacts of each N—O group (i.e., N—O not participating in H-bonding) with hydrogens lead to weak FM (along the chain) and weak AFM (between the chains) coupling pathways due to the comparable interatomic distances, where the product of spin densities $\rho_{N-O}\rho_H$ is not very significant due to the smaller spin density of the hydrogens but in our case cannot be ignored. It is clear from the correlation of the magnetic (Faraday, ESR, and NMR) data with the crystallographic data that the dominant interaction is antiferromagnetic in both chains (**3** and **4**) mainly

through the N—**O···H**—C≡C— H-bonding pathway along the chains and also due to the close interchain N—**O···O**—N contacts.

Conclusion

It is important to re-emphasize here that the determination of both magnitude and sign of spin densities in a *randomly distributed molecule* in solution medium is necessary to correlate the bulk magnetic behavior of the *well ordered hydrogen-bonded systems* in molecular crystals. More importantly, it is vital to identify the spin densities of the H-bonding active sites (donor···acceptor) of an isolated molecule in solution. In our present systems **3** and **4** (N—O···H—C≡C—), the active sites were well analyzed in order to determine both the sign and magnitude of spin density distribution by comparing both paramagnetic NMR and ESR spectroscopic data. Earlier, Romero et al. have shown by ab initio calculation that both meta- and para-pyridine ethynyl based nitronylnitroxide systems have no spin densities on the acetylenic protons even though the *spin density transfer* in the solid state was well documented by polarized neutron diffraction studies performed on single crystals in the same work.[5] Our experimental results show that both para-phenyl ethynyl and para-pyridine ethynyl based nitronylnitroxide systems **3** and **4**, respectively, have positive spin densities at the acetylenic H-bonding donor site in a randomly oriented molecular environment, where the probability of *spin density* transfer is negligible. These results unambiguously support the idea that the major AFM coupling pathway is indeed mediated through N—**O···H**—C≡C— type H-bond contacts along the one-dimensional chain of the molecule in the crystalline state, although the other contacts (e.g., N—**O···O**—N) between the chains also contribute to the overall magnetic properties.

Experimental Section

2,3-Dimethyl-2,3-bis(hydroxylamino)-butane sulfate salt was obtained from Acros Organics. All other chemicals were obtained from Aldrich. All of the reactions were followed by thin-layer chromatography carried out on 0.25 mm ALUGRAM SIL G/ UV254 silica gel plates using a UV detector. Column chromatography was performed on silica gel (E. Merck, 230−400 mesh). Purification of radical **3** was done on PLC plates (200 × 200 mm) silica gel 60 F_{524} with concentrating zone (200 × 4 mm). ^{1}H NMR and ^{13}C NMR spectra were recorded on Bruker DPX 250 spectrometers with solvent proton or carbon signal as internal standards. ^{1}H NMR spectra of the paramagnetic sample were recorded on a Bruker DPX 300 spectrometer with solvent proton as an internal standard. Chemical shifts are given in ppm relative to the signal of $CDCl_3$ which was taken as $\delta = 7.26$ (for ^{1}H). UV−vis spectra were recorded with a Perkin-Elmer spectrometer (UV−vis/NIR Lambda 900). FAB mass spectra of radicals were obtained on a ZAB-2 mass spectrometer. Infrared spectra were recorded using KBr pressed pellets on a Nicolet 730 FTIR spectrometer. The X-ray crystallographic data were collected on a Nonius Kappa CCD (Mo Kα) diffractometer equipped with a graphite monochromator. The structures were solved by the direct method and refined by a full-matrix least-squares procedure. ESR spectra were recorded on a CW X-band ESP 300 instrument equipped with an NMR gauss meter (Bruker ER035), a frequency counter (Bruker ER 041 XK), and a variable temperature control continuous flow N_2 cryostat (Bruker B-VT 2000). Melting points were measured on Büchi B-545 apparatus and are uncorrected. Temperature-dependent static susceptibilities of powdered crystalline samples were recorded using a Faraday-type magnetometer in the temperature range 4.5−300 K. The measurements presented were done using a computer controlled Cahn D-200 microbalance and a Bruker B-MN 200/60 power supply. The diamagnetic corrections of the molar magnetic susceptibilities were applied using well-known Pascal's constants.

5-Ethynyl-pyridine-2-carbaldehyde (10). A mixture of compound **9** (300 mg, 1.47 mmol) and K_2CO_3 (100 mg) was stirred in methanol (10 mL) for 3 h at room temperature under an argon atmosphere. The solvent was evaporated, and the solid was dissolved in dichloromethane (20 mL) and washed with $NaHCO_3$ (10 mL) solution (1 g in 10 mL). Evaporation of the organic layer gave a yellow product (**10**). Yield: 0.134 g (70%).

^{1}H NMR (250 MHz, DMSO-d_6, RT) δ: 9.97 (s, 1H, —CHO), 8.89 (s, 1H, Py-H_6), 8.14 (d, 1H, ^3J = 7.75 Hz, Py-H_4), 7.91 (d, 1H, ^3J = 7.90 Hz, Py-H_3), 3.34 (s, 1H, C≡H). ^{13}C NMR (62.5 MHz, DMSO-d_6, RT) δ: 192.75 (C═O), 152.49 (Py-C_6), 151.07 (Py-C_1), 140.45 (Py-C_4), 122.99 (Py-C_5), 121.25 (Py-C_6), 87.52 (C≡C), 79.9 (C≡C). FTIR (KBr disk; ν in cm^{-1}): 3186 (vs, C≡C—H stretching), 2104 (vs, C≡C), 1689 (vs, —CHO) ppm. R_f (in $CHCl_3$) ∼ 0.40. mp: 121−122 °C.

2-(5-Ethynyl-2-pyridyl)-4,4,5,5-tetramethyl-imidazoline-1,3-diol (11). A mixture of **10** (70 mg, 0.53 mmol) and 2,3-dimethyl-2,3-bis(hydroxylamino)-butane (0.100 g, 0.67 mmol) was stirred in methanol (10 mL) at room temperature under an argon atmosphere. The clear methanol solution turned turbid after 3 days. The solvent from the flask was evaporated under reduced pressure, and the obtained yellow powder was washed with petroleum ether (bp 40−65 °C) to remove the unreacted aldehydes to afford bright yellow powder (**11**). Yield: 0.1 g (72%).

^{1}H NMR (250 MHz, DMSO-d_6, RT) δ: 8.58 (s, 1H); 7.89 (dd, 1H, ^4J = 1.9 Hz, ^3J = 8.2 Hz); 7.78 (s, 2H, —OH); 7.6 (d, 1H,^3J = 8.21 Hz); 4.64 (s, 1H, imidazoline —CH); 3.16 (s, 1H, C≡CH); 1.06 (s, 12H, —CH_3) ppm. ^{13}C NMR (62.5 MHz, DMSO-d_6, RT) δ: 161.54 (C2); 150.56 (C6); 138.96 (C4); 122.12 (C3); 117.51 (C5); 90.99 (imidazoline —CH); 83.67 (C≡C); 80.71 (C≡C); 66.50 (imidazoline —C—$(CH_3)_2$); 24.01 (—CH_3); 17.44 (—CH_3).

2-(5-Ethynyl-2-pyridyl)-4,4,5,5-tetramethylimidazoline-1,3-oxyl (4). Compound **11** (90 mg, 0.345 mmol) was suspended in a chloroform/water two-phase mixture (20 mL each). The mixture was cooled in an ice bath, and solid $NaIO_4$ (74 mg, 0.345 mmol) was added into the flask with rapid stirring for 5 min. The formed blue-colored organic layer was separated, and the aqueous layer was extracted with dichloromethane (5 mL) to remove the rest of the blue organic part completely. The combined organic layer was dried over $MgSO_4$ and purified using chromatography (silica, acetone, R_f ∼ 0.8) to yield a blue solid product, **4**. Single crystals were obtained by slow evaporation from a petroleum ether/acetone mixture (5:2). Yield: 0.53 mg (60%).

EPR (in toluene/isopropanol, $c \sim 5 \times 10^{-5}$ M, RT, ν = 9.410277 GHz, 0.5 mW power, 6 scans): Five lines, g_{iso} = 2.0068, a_N = 7.44 G. FAB MS: *m*/*z* 259. UV−vis (in $CHCl_3$): 588 nm (ϵ = 166 M^{-1} cm^{-1}), 387 nm (ϵ = 8332 M^{-1} cm^{-1}). FTIR (KBr disk; ν in cm^{-1}): 3199 (vs, C≡CH stretching), 2102 (w, C≡C), 1367 (s, N—O), 837 (s, C—H out-of-plane deformation).

2-(4-Ethynyl-phenyl)-4,4,5,5-teramethyl-imidazolidine-1,3-diol (7). 4-Ethynylbenzaldehyde (300 mg, 2.3 mmol) and 2,3-dimethyl-2,3-bis(hydroxylamino)-butane (375 mg, 2.5 mmol) were suspended in methanol (15 mL) under argon and stirred for 4 days at room temperature. The formed white precipitate was filtered to give **7**. Yield: 0.140 g (23%).

^{1}H NMR (250 MHz, DMSO-d_6, RT) δ: 7.8 (s, 2H, −OH); 7.45 (dd, 4H); 4.49 (s, 1H, imidazoline −CH); 4.43 (s, 1H, C≡CH); 1.06 (s, 6H, $-CH_3$); 1.02 (s, 6H, $-CH_3$).

2-(5-Ethynyl-2-phenyl)-4,4,5,5-tetramethylimidazoline-1,3-oxyl (3). Compound **7** (100 mg, 0.388 mmol) was suspended in a chloroform/water two-phase mixture (10 mL each). Solid $NaIO_4$ (100 mg, 0.405 mmol) was added into the flask and stirred for 5 min. The formed dark blue organic layer was separated, dried over $MgSO_4$, and filtered. The blue powder was purified by preparative thin-layer chromatography using a 1:1 ratio of an acetone/hexane mixture ($R_f \sim 0.88$) and recrystallized at room temperature in an acetone/petroleum ether (1:1) mixture to yield blue-colored needles (**3**). Yield: 40 mg (40%).

EPR (in toluene/isopropanol, $c \sim 10^{-4}$ M, RT, $\nu = 9.412\,969$ GHz, 0.5 mW power, 6 scans): Five lines, $g_{iso} = 2.0068$, $a_N = 7.47$ G. FAB MS: *m*/*z* 258. UV−vis ($CHCl_3$): 610 nm ($\epsilon = 280\ M^{-1}\ cm^{-1}$), 378 nm ($\epsilon = 11\,165\ M^{-1}\ cm^{-1}$). FTIR (KBr disk, ν in cm^{-1}): 3214 (s, ≡C−H), 2993 (ms, Si−CH), 2098 (ms, C≡C), 1363 (s, N−O), 837 (C−H out-of-plane deformation).

Acknowledgment. We thank Prof. Dr. W. Haase and Dr. K. Falk (TU - Darmstadt) for the magnetic measurements. This work was supported by DFG.

Supporting Information Available: EPR and UV−vis spectra of **3** and **4**, EPR susceptibility data of **3**, and crystallographic data of **3** and **4**. The X-ray crystallographic data has been deposited with the Cambridge Crystallographic Data Centre (CCDC Nos. 273738 and 273739) for compounds **3** and **4**, respectively. Copies of this information can be obtained free of charge from The Director, CCDC, 12 Union Road, Cambridge,CB21EZ,U.K.(fax,+441223336033;e-mail,deposit@ccdc.cam.ac.uk).

References and Notes

(1) (a) Sugawara, T.; Nakazaki, J.; Matsushita, M. M. In *Magnetic properties of Organic Materials*; Lahti, P. M., Ed.; Marcel Dekker: New York, 1999; Chapter 26, pp 540−545. (b) Kahn, O. *Molecular Magnetism*; VCH: New York, 1993. (c) Miller, J. S., Drillon, M., Eds. *Magnetism: Molecules to Materials*; Wiley-VCH: Weinheim, Germany, 2001−2003; Vols. I−IV. (d) Rajca, A. *Chem. Rev.* **1994**, *94*, 871. (e) Tamura, M.; Nakazawa, Y.; Shiomi, D.; Nozawa, K.; Hosokoshi, Y.; Ishikawa, M.; Takahashi, M.; Kinoshita, M. *Chem. Phys. Lett.* **1991**, *186*, 401. (f) Kinoshita, M. *Jpn. J. Appl. Phys.* **1994**, *33*, 5718. (g) Rajca, A.; Wongsriratanakul, J.; Rajca, S. *Science* **2001**, *294*, 1503. (h) Rajca, A.; Rajca, S.; Wongsriratanakul, J. *J. Am. Chem. Soc.* **1999**, *121*, 6308. (i) Rajca, A.; Wongsriratanakula, J.; Rajca, S.; Cerny, R. L. *Chem.—Eur. J.* **2004**, *10*, 3144. (j) Rajca, A. *Adv. Phys. Org. Chem.* **2005**, *40*, 153−199.

(2) (a) Sugawara, T.; Matsushita, M. M.; Izuoka, A.; Wada, N.; Takeda, N.; Ishikawa, M. *J. Chem. Soc., Chem. Commun.* **1994**, 1723. (b) Awaga, K.; Okuno, A.; Yamaguchi, A.; Hasegawa, M.; Inabe, T.; Maruyama, Y.; Wada, N. *Phys. Rev. B* **1994**, *49*, 3975.

(3) (a) Cirujeda, J.; Hernández-Gasió, E.; Rovira, C.; Stranger, J. -L.; Turek, P.; Veciana, J. *J. Mater. Chem.* **1995**, *5*, 243−252. (b) Catala, L.; Feher, R.; Amabilino, D. B.; Wurst, K.; Veciana, J. *Polyhedron* **2001**, *20*, 1563. (c) Turek, P.; Nozawa, D.; Shiomi, K.; Awaga, K.; Inabe, T.; Maruyama, Y.; Kinoshita, M. *Chem. Phys. Lett.* **1991**, *180*, 327.

(4) (a) Ferrer, J. R.; Lahti, P. M.; George, C.; Oliete, P.; Julier, M.; Palacio, F. *Chem. Mater.* **2001**, *13*, 2447. (b) Field, L. M.; Lahti, P. M. *Chem. Mater.* **2003**, *15*, 2861.

(5) Romero, F. M.; Ziessel, R.; Bonnet, M.; Pontillon, Y.; Ressouche, E.; Schweizer, J.; Delley, B.; Grand, A.; Paulsen, C. *J. Am. Chem. Soc.* **2000**, *122*, 1298.

(6) Romero, F. M.; Ziessel, R.; Drillon, M.; Tholence, J. L.; Paulsen, C.; Kyritsakas, N.; Fisher, J. *Adv. Mater.* **1996**, *8*, 826.

(7) Matsushita, M. M.; Izuoka, A.; Sugawara, T.; Kobayashi, T.; Wada, N.; Takeda, N.; Ishikawa, M. *J. Am. Chem. Soc.* **1997**, *119*, 4369.

(8) (a) Zhang, J.; Baumgarten, M. *Chem. Phys.* **1997**, *222*, 1. (b) Ali, M. D.; Vyas, S.; Datta, S. N. *J. Phys. Chem. A* **2005**, *109*, 6272.

(9) Hosokoshi, Y.; Katoh, K.; Nakazawa, Y.; Nakano, H.; Inoue, K. *J. Am. Chem. Soc.* **2001**, *123*, 7921−7922.

(10) Hicks, R. G.; Lemaire, M. T.; Öhrström, L.; Richardson, J. F.; Thompson, L. K.; Xu, Z. *J. Am. Chem. Soc.* **2001**, *123*, 7154.

(11) Rajadurai, C.; Fuhr, O.; Enkelmann, V.; Baumgarten, M. *J. Phys. Org. Chem.* **2006**, *19*, 257−262.

(12) Desiraju, G. R. *Crystal Engineering. The Design of Organic Solids*; Elsevier: Amsterdam, The Netherlands, 1989.

(13) Weil, J. A.; Bolton, J. R.; Wertz, J. E. *Electron Paramagnetic Resonance*; John Wiley & Sons: New York, 1994.

(14) Cirujeda, J.; Gancedo, J. -V.; Jürgens, O.; Mota, F.; Novoa, J. J.; Rovira, C.; Veciana, J. *J. Am. Chem. Soc.* **2000**, *122*, 11393.

(15) Takui, T.; Miura, Y.; Inui, K.; Teki, Y.; Inoue, M.; Itoh, K. *Mol. Cryst. Liq. Cryst.* **1995**, *271*, 55.

(16) Hirel, C.; Pécaut, J.; Choua, S.; Turek, P.; Amabilino, D. B.; Veciana, J.; Rey, P. *Eur. J. Org. Chem.* **2005**, 348.

(17) (a) Kreilick, R. E.; Becker, J.; Ullman, E. F. *J. Am. Chem. Soc.* **1969**, *91*, 5121. (b) Davis, M. S.; Morokuma, K.; Kreilick, R. E. *J. Am. Chem. Soc.* **1972**, *94*, 5588.

(18) Jesson, J. P. *J. Chem. Phys.* **1967**, *47*, 579.

(19) Goldman, J.; Peterson, T. E.; Torssell, K.; Becker, J. *Tetrahedron* **1973**, *29*, 3833.

(20) (a) Heise, H.; Köhler, F. H.; Mota, F.; Novoa, J. J.; Veciana, J. *J. Am. Chem. Soc.* **1999**, *121*, 9659. (b) Rancurel, C.; Heise, H.; Köhler, F. H.; Schatzschneider, U.; Rentschler, E.; Gancedo, J. V.; Veciana, J.; Sutter, J.-P. *J. Phys. Chem. A* **2004**, *108*, 5903 and references therein.

(21) (a) Deumal, M.; Cirujeda, J.; Veciana, J.; Novoa, J. J. *Adv. Mater.* **1998**, *10*, 1461. (b) Deumal, M.; Novoa, J. J.; Bearpark, M. J.; Celani, P.; Olivucci, M.; Robb, M. A. *J. Phys. Chem. A* **1998**, *102*, 8404.

(22) Deumal, M.; Cirujeda, J.; Veciana, J.; Novoa, J. J. *Chem.—Eur. J.* **1999**, *5*, 1631.

(23) Sonogashira, K.; Tohada, Y.; Hagihara, N. *Tetrahedron Lett.* **1975**, 4470.

(24) Osiecki, J. H.; Ullman, E. F. *J. Am. Chem. Soc.* **1968**, *90*, 1078.

(25) (a) Rajadurai, C.; Ivanova, A.; Enkelmann, V.; Baumgarten, M. *J. Org. Chem.* **2003**, *68*, 9907. (b) Rajadurai, C.; Ostrovsky, S.; Falk, K.; Enkelmann, V.; Haase, W.; Baumgarten. M. *Inorg. Chim. Acta* **2004**, *357*, 581.

(26) Wautelet, P.; Moigne, J. L.; Videva, V.; Turek, P. *J. Org. Chem.* **2003**, *68*, 8025.

(27) The solution ESR spectra were simulated using the Bruker WINEPR - SimFonia programme.

(28) (a) Bleaney, B.; Bowers, K.; *Proc. R. Soc. London* **1952**, *A214*, 451. (b) Yoshida, K. *Theory of Magnetism*; Springer: Berlin, Heidelberg, New York, 1998. (c) Kahn, O., Ed. *Magnetism: A Supramolecular Function*; Kluwer: Dordrecht, The Netherlands, 1996.

(29) McConnell, H. M. *J. Chem. Phys.* **1963**, *39*, 1916.